Journal of Constructional Steel Research 147 (2018) 293–312

Contents lists available at ScienceDirect

Journal of Constructional Steel Research

Experimental buckling behaviour of web tapered I-section steel columns

Trayana Tankova *, João Pedro Martins, Luís Simões da Silva, Rui Simões, Helder D. Craveiro

ISISE – Department of Civil Engineering, University of Coimbra, Coimbra, Portugal

ARTICLE INFO

Article history:
Received 9 January 2018
Received in revised form 5 March 2018
Accepted 15 April 2018
Available online xxxx

Keywords:
Columns
Stability
Steel
Eurocode 3
Tapered members
Experimental tests

ABSTRACT

Tapered steel members offer a better cross-section utilization along the member, which makes them an interesting and more economical alternative to prismatic ones. Yet, the design methodologies available do not provide a clear and sufficient guidance for the stability verification of such members.
Alternatively, nowadays, the existing computer capacity and software programs provide an accessible and rapid means of reproducing the structural performance of members and systems, although they require beforehand validation to assure the plausibility of their predictions. For that, a full-scale experimental programme on non-uniform members was carried out, covering column, beam and beam-column tests. The test results are used to validate a numerical model commonly used for the assessment of stability design rules.
In this paper, firstly, a global overview of the experimental tests is presented, which covers the test layout, member dimensions and the supplementary tests, essentially characterization of material properties, geometrical dimensions and imperfections, and residual stresses. The key results from each experiment are presented and discussed, they are further compared with numerical and analytical estimations of the member resistance. Finally, the experimental results provide physical validation of the design method proposed in Marques et al. (2012) for web-tapered columns.

1. Introduction

Several practical applications of steel members do not fully exploit the capacity of their cross-section along the length. In fact, in almost all applications, the design internal forces are not constant and assuming constant resistant properties along the length (i.e. constant cross-section) is often not the optimal structural arrangement, especially for large span structures. An efficient solution is, therefore, to vary the member dimensions along its length by adjusting them to the demand for cross-section resistance. The most straight forward application are columns with stepped section, more aesthetical applications are tapered members, either with varying depth and/or flange widths. Moreover, members with irregular distribution of restraints can also be classified as non-uniform. (Fig. 1).

Often, in practice, due to architectural reasons either related to the functional performance of the building or driven by aesthetic criteria, it is not possible to have regular structures which further increases the need for an efficient design of irregular structures. From a fabrication point of view, non-uniform members are seen as competitive since, nowadays, automatic welding processes of steel plates is an economical manufacturing process. However, as in any other structural solution, these advantages depend directly upon the correct use of suitable tools (numerical, analytical and/or code-like formulae) by the designer. In this sense, it is highlighted the lack of design rules, guidance and validated solution for non-uniform members.

Therefore, having the aim of providing practical solutions, and acknowledging the fact that experimental results are crucial for the correct characterization of the real behaviour of tapered steel members, this paper presents the results of four full-scale experiments on web tapered columns and a beam-column carried out by the authors. Additionally, these experimental results are further used for the calibration and validation of the numerical [2] and analytical [5] models for the flexural and lateral-torsional buckling resistance of tapered beam-columns. Finally, regarding the stability behaviour, it is noted that the characterization of imperfections (geometric and residual stresses) is essential. In fact, these imperfections are known to be the main source of discrepancies between theoretical and real values of the load carrying capacity of steel members. Therefore, these imperfections were measured and taken into account during the calibration of the numerical model.

2. Tapered columns: analytical and experimental work by others

Due to the possible economic advantages, the buckling behaviour of non-uniform columns has attracted the interest of researchers since the last century. At first, contributions were focused on analytical solutions for the elastic critical behaviour of such members.

* Corresponding author at: Department of Civil Engineering, University of Coimbra, Polo II, Pinhal de Marrocos, 3030-290 Coimbra, Portugal.
E-mail address: ttankova@uc.pt (T. Tankova).

https://doi.org/10.1016/j.jcsr.2018.04.015
0143-974X/

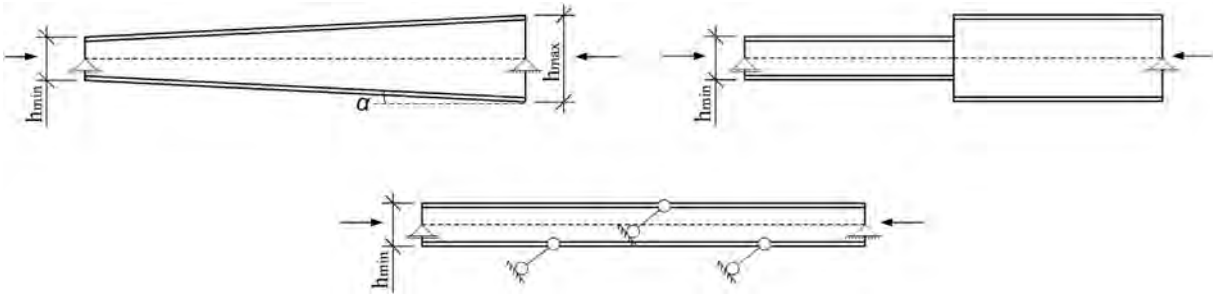

Fig. 1. Non-uniform members.

Timoshenko & Gere [6] proposed numerical solutions of the differential equations for the determination of critical loads for stepped columns and bars with linearly varying cross-section. The proposed solutions are given in the following form:

$$P_{cr} = m\frac{EI_{\max}}{L^2} \tag{1}$$

where the factor m is a tabulated value depending on the ratio between the minimum and the maximum moments of inertia and the ratio between the lengths of the column segments. The solution for members with linearly varying cross-section is given in the same format, whereby the tabulated values of m depend only on the ratio between the minimum and the maximum moments of inertia. A similar approach for was used for the calibration of a solution for tapered columns under stepped loading profile in [7].

Another approach, proposed by *Lee* et al. [4,8], is based on a modification factor g of the tapered member length which transforms it into an equivalent prismatic member with a uniform cross-section equal to the shallow tapered member end, as shown on Fig. 2. The critical load is then calculated based on the shallow cross-section Eq. (2) and the g factor was calibrated as a function of the taper ratio γ, Eq. (3).

$$P_{cr} = \frac{\pi^2 EI_{\min}}{(gL)^2} \tag{2}$$

$$g = 1-0.375\gamma + 0.08\gamma^2(1-0.0775\gamma) \tag{3}$$

where for linearly tapered member γ defines the cross-section height h_i at any distance x from the smaller end as

$$h_i = h_{min}\left(1+\frac{x}{L}\gamma\right) \tag{4}$$

Ermopoulos [10] established the elastic non-linear equilibrium equations of non-uniform members in frames under compression for non-sway and sway modes. These equations were solved using an iterative procedure and the corresponding critical loads and equivalent length factors were presented in forms of tables and graphs similar to the classical effective length graphs by *Wood* [11].

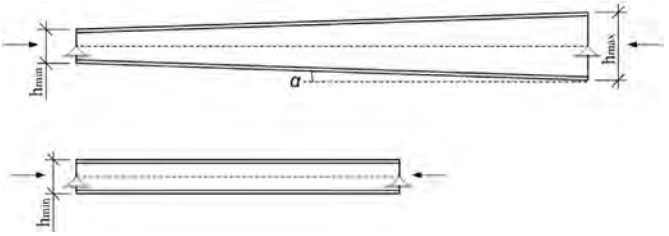

Fig. 2. Equivalent prismatic member.

Hirt & Crisinel [12] proposed an expression for determination of an equivalent moment of inertia of tapered columns, I_{eq}, with I-shaped cross sections, depending on the type of web variation:

$$P_{cr} = \frac{\pi^2 EI_{\text{eq}}}{(L)^2} \tag{5}$$

with

$$I_{eq} = CI_{y,\max} \quad C = 0.08 + 0.92r \quad r = \sqrt{\frac{I_{y,\min}}{I_{y,\max}}} \tag{6}$$

Marques (2012) derived closed-form expressions for the critical load of web-tapered columns:

$$N_{cr,Tap} = A\cdot N_{cr,\min} \rightarrow A = \gamma_I^{0.56}\left(1-0.04\cdot\tan^{-1}(\gamma_I-1)\right)$$
$$\gamma_I = I_{y.\max}/I_{y.\min} \tag{7}$$

Concerning the ultimate resistance of non-uniform columns, some studies were carried out. *Salter* et al. [9] carried out tests on web-tapered steel columns. The specimens were loaded in axial compression and major axis bending moment. In total, eight tests were performed. In three of the tests, lateral restraint was provided to one flange at mid-height. The initial out-of-straightness was measured only for the minor column axis and was comparatively high. The specimens were about half to one third of their full size. The test results were compared with numerical non-linear analyses for which good agreement was reported. Regarding the code estimations for the resistance of such columns, the authors concluded that they were safe sided with possibility for improvement.

Baptista & Muzeau [13] adjusted the Eurocode 3 design rules for flexural buckling of columns to tapered members by an additional coefficient k. This coefficient was calibrated numerically and given in the form of an abacus, is applied to the reduction factor of a column with the smallest cross section.

Raftoyiannis & Ermopoulos [14] proposed an analytical formulation based on the differential equation of imperfect linearly tapered and

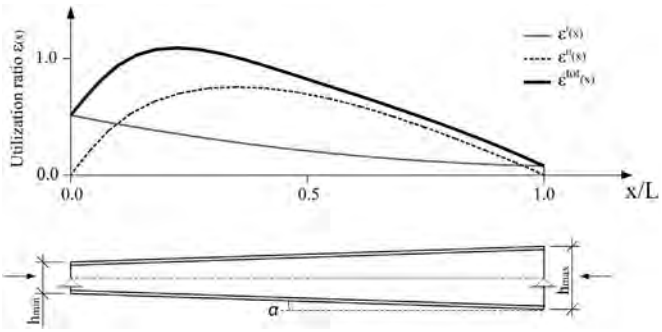

Fig. 3. Utilization ratio: non-uniform members.

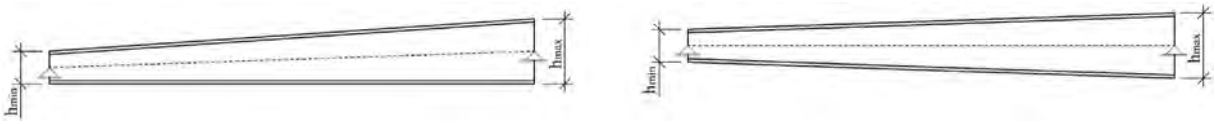

Fig. 4. a) "L"-shape tapered member; b) "V"-shape tapered member.

Table 1
Experimental programme.

Member	γ_h	Shape	h_{min}	h_{max}	b_{top}	b_{bot}	t_w	$t_{f,top}$	$t_{f,bot}$	L
–	–		mm	mm	mm	mm	mm	mm	mm	m
C1	4	V	120 (121)	480 (482)	100 (102)	100 (102)	12 (12.5)	12 (12.4)	12 (12.7)	6
C2	2	V	185 (186)	370 (372)	110 (112)	110 (113)	6 (5.95)	12 (12.4)	12 (12.6)	6
C3	3	L	120 (120)	360 (357)	100 (100)	100 (100)	10 (10.1)	16 (16.5)	16 (16.1)	6
BC	3	L	120 (120)	360 (357)	100 (100)	100 (103)	10 (11.1)	16 (16.2)	16 (16.9)	6

All specimens were fabricated in steel grade S355 JR + M using welded hot-rolled plates according to EN 10025-2:2004 (+M) [8].

stepped columns subject to axial force. The initial geometrical imperfection was considered with a parabolic shape using the magnitudes proposed in Eurocode 3. The proposed design method is then formed on a yield criterion which shall be verified at several locations along the column. The proposed method was compared to advanced numerical simulations and satisfactory correlation was found.

In *Naumes* [16] the equilibrium equation for flexural buckling of tapered members was also established. In this derivation, the shape of the initial imperfection was considered eigenmode conform. It was shown that the Ayrton-Perry design format can be adopted for the design of non-uniform members. However, the proposed expressions are not applicable for practical design verification due to lack of recommendations for the determination of the design location.

In [17], *Kim* developed a design rule for web-tapered members according to the AISC (2010) [18] design rules based on an equivalent prismatic member with the same first order resistance and elastic critical load.

Furthermore, in [2], *Marques* et al. proposed new design rules for the verification of flexural buckling resistance of tapered members, consistent with EN 1993-1-1 [1]. In this model, eigenmode conform imperfections were considered for the second order forces, Fig. 3, leading to similar equations as those presented in EN 1993-1-1 [1] for the stability verification of prismatic columns.

As a result, as long as a second order failure location is known and an additional imperfection factor is considered to account for the non-uniformity either of the loading or of the cross section, the verification may be performed analogously to the rules for prismatic columns. This second order failure location and additional imperfection factor were replaced in some of the terms by an "over-strength" factor φ, which is given for a set of tapered ratios. This approach only requires the determination of the location where the stresses due to the applied forces are maximum, which is a straight-forward procedure.

Regarding the behaviour of members loaded in combination of bending and compression, in 1963, *Butler & Anderson* [19] carried out experimental tests on the elastic stability of tapered beam-columns. As a continuation of the work by *Butler* [19], in [20] the authors performed an experimental study where fifteen tapered I-section members were tested in bending and in a combination of bending and compression. The tested members were chosen to fail in the inelastic range. These experiments assessed the difference in the resistance of members manufactured using different fabrication procedures. In [21], *Shiomi* et al. reported on an experimental programme on tapered beam-columns which aimed at the characterization of the structural behaviour of such members for the development of a design formulation.

Buckling and stability non-linear analysis of tapered members and/or structures consisting of tapered members are found in [22,23,24,25]. The most recent studies for tapered steel members are mostly based on analytical work which is validated by advanced non-linear numerical simulations [2,3,17].

The design rules for tapered columns and beams developed in [2,3] were used to propose a verification format for the stability verification of web-tapered beam-columns [5]. The interaction formulae in EC3-1-1 for prismatic members were adapted for tapered members, validated through extensive FEM numerical simulations covering several combinations of bending moment about strong axis, My, and axial force, N, and levels of taper.

3. Experimental tests on web-tapered steel columns

3.1. Introduction

In order to characterize the buckling behaviour of web-tapered steel columns, full scale tests were carried out at the University of Coimbra in the framework of the research project TAPERSTEEL PTDC/ECM-EST/1970/2012. Its objective was to study the stability behaviour of non-uniform steel members. The experimental programme covered different stability phenomena – flexural buckling of columns under uniform compression, lateral-torsional buckling of non-uniform beams under linearly varying bending moment and lateral-torsional buckling of beam-columns loaded with major axis bending moment and uniform compressive force. In the following sections the results from the column and beam-column tests are presented and discussed.

3.2. Geometry, boundary conditions and layout

All specimens were web-tapered, with different tapering ratios, and two different shape configurations were used: i) different inclination of each flange with respect to the centroid of the beam (shape L Fig. 4a); ii) the equal flange inclination with respect to its centroidal axis (shape V Fig. 4b). The nominal and measured (values in brackets) dimensions of the tested members are summarized in Table 1.

Table 2
Cross-section classification of column members.

Cross-section class	Column 1	Column 2	Column 3
1	[0; 0.59L]	–	[0; 0.67L]
2	(0.59L; 0.71L]	[0; 0.05L]	(0.67L; 0.83L]
3	(0.71L; 0.82L]	(0.05; 0.14 L]	(0.83 L; 0.95 L]
4	(0.82L; L]	(0.14 L; L]	(0.95 L; L]

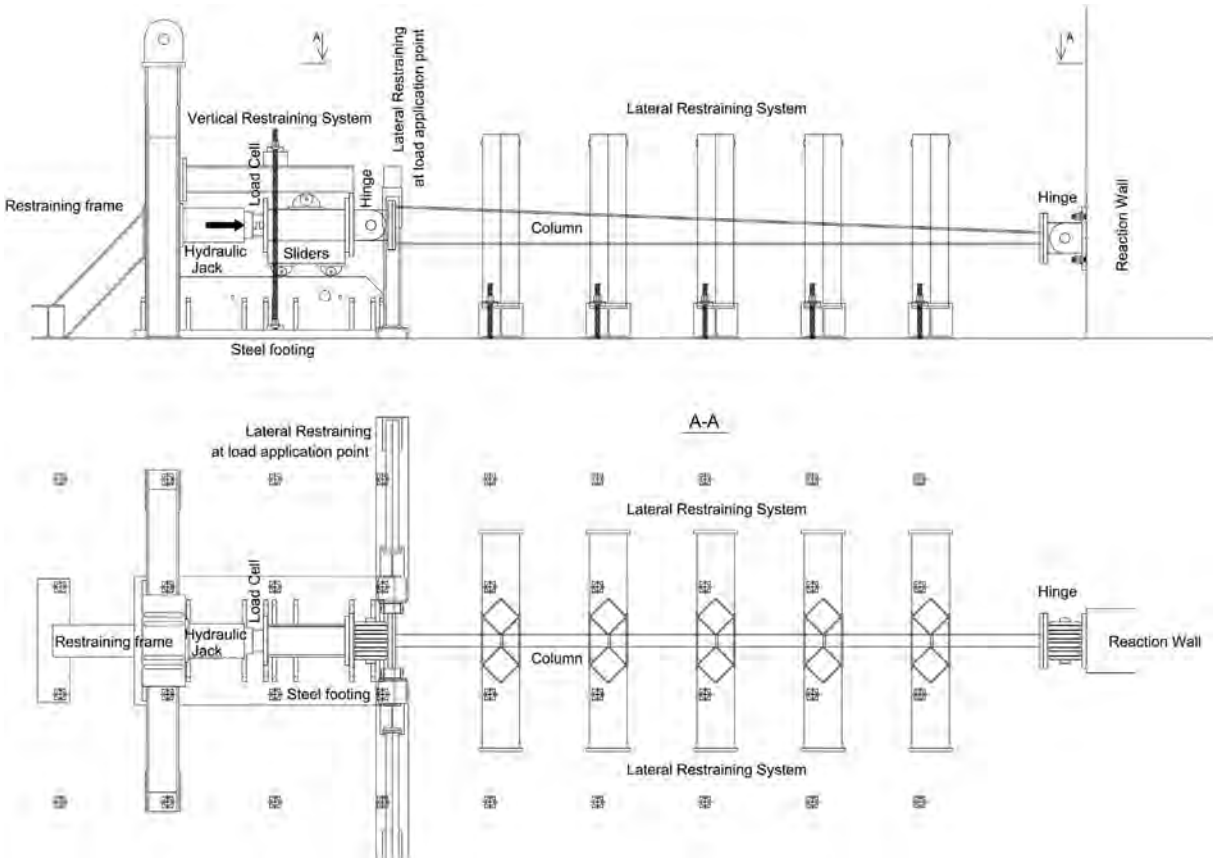

Fig. 5. Test layout, Column 3 (and identical for the other columns).

3.2.1. Column tests

Three column tests were carried out. The specimens were designed to assess their in-plane flexural buckling behaviour, being the relevant parameter in the design of non-uniform members. Another aspect was the cross-section variation along the member length. Table 2 and Fig. 7 summarize the variation of the cross-section class along the member length (L) for the three specimens. In C1 approximately 18% of the member was in class 4, for C2 86% and 5% for C3, respectively.

The tested specimens had different taper ratios (2, 3 and 4, respectively), but the same length of 6 m. The three columns were tested using the layout shown in Fig. 5. They were simply supported on both ends using pinned connections (Fig. 6a), which allowed the free rotation in the plane of the column. At the point of load application, the vertical and transversal movements of the columns were restrained (Fig. 6b). The global out-of-plane buckling was prevented by the implementation of lateral restraints at each meter length of the column (5 in total), Fig. 6c.

The lateral restraints along each member were implemented using vertical SHS 250 × 10 profiles rotated by 45° with the edge aligned with the members' top and bottom flanges (Fig. 6c). The SHS 250 × 10 profiles are connected at their bases to a horizontal profile attached to the strong floor and at their top welded to a plate connecting both sides.

Strains were measured using strain-gauges type FLA-6-11 glued to the web and the flanges. On the web, they were positioned along vertical lines (3 or 4 at each cross-section), and three strain gauges on each flange (top and bottom). For the measurement of vertical and lateral displacements during the experiment, LVDTs (linear variable differential transducers) were installed at several locations along the columns,

a) Pinned connection

b) Lateral bracing at support

c) Lateral restraints

Fig. 6. Supports.

their position for the three column specimens is shown in Fig. 7. The positions of measurement of vertical displacements are marked with *V* and the horizontal with *H*, respectively.

3.2.2. Beam-column test

For the validation of the design rules for beam-columns, the last test performed was on a member loaded in bending and compression. The specimen had the exact same dimensions as column C3, thus allowing for a better comparison of the obtained resistance.

In this experiment, it was meant to validate the lateral-torsional buckling of a beam-column loaded with axial force and major axis bending moment. The load was applied with eccentricity (Fig. 8), allowing for proportional increase of the bending moment and the axial force. The test layout is shown on Fig. 9, where the member was restrained laterally at mid-span. At the shallow end the specimen was connected to the reaction wall through a pinned connection, which allowed free rotation out-of-plane. At the deepest section where there was a welded cantilever section which served for the load application, it was vertically and laterally restrained.

The vertical and horizontal displacements were measured at each meter of length of the member (V1 to V5 and H2, H4, H7, H9). Additional measurements were obtained at the expected critical locations at axis B and E, where the horizontal displacements were measured at the level of the flanges as well.

3.3. Complementary tests

3.3.1. Characterization of material properties

The test specimens were fabricated by welding of hot-rolled steel plates fabricated according to EN 10025-2:2004 [32]. The steel grade of these steel plates is S355 ($f_{y,nom} = 355$ MPa) and the steel quality is JR. The steel grade of all additional plates used to fabricate the hinges is the same or higher and the steel used for the pins and bolts (M30, Grade A, EN 15048-1 [33] and EN ISO 4017 [34]) is high strength steel, class 8.8 ($f_{y,nom} = 640$ MPa). The nuts and washers required for the bolts are also Grade A, in accordance with the standards EN ISO 4032 [35] and EN ISO 7089 [36], respectively.

The complete characterization of the experiments requires the determination of the actual material properties. For that, standard coupons were extracted from each specimen and subjected to tension in order to characterize their material properties. A total of six coupons were milled from each specimen: three from flanges and three from the

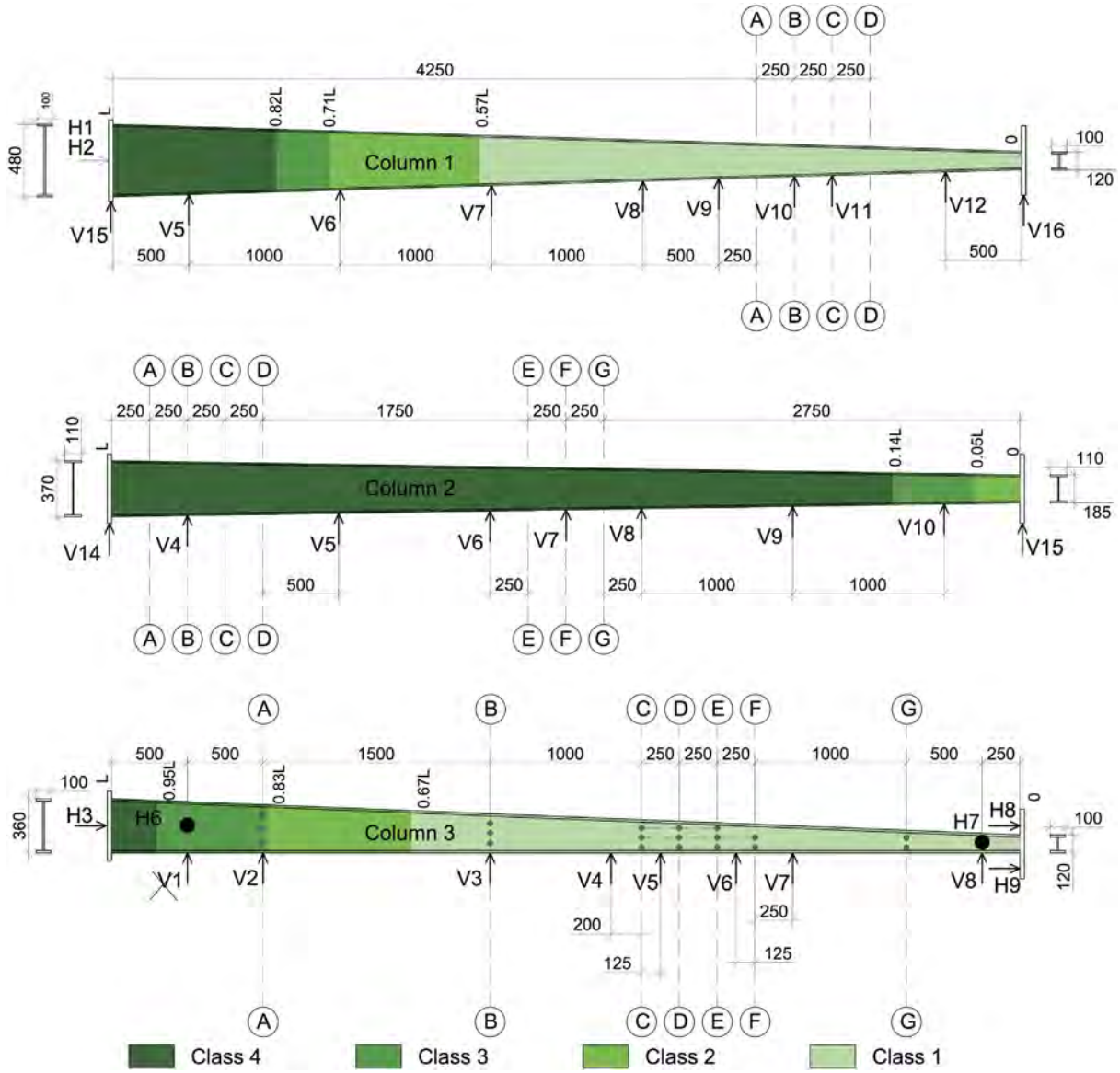

Fig. 7. Plan of LVDTs and strain gauges.

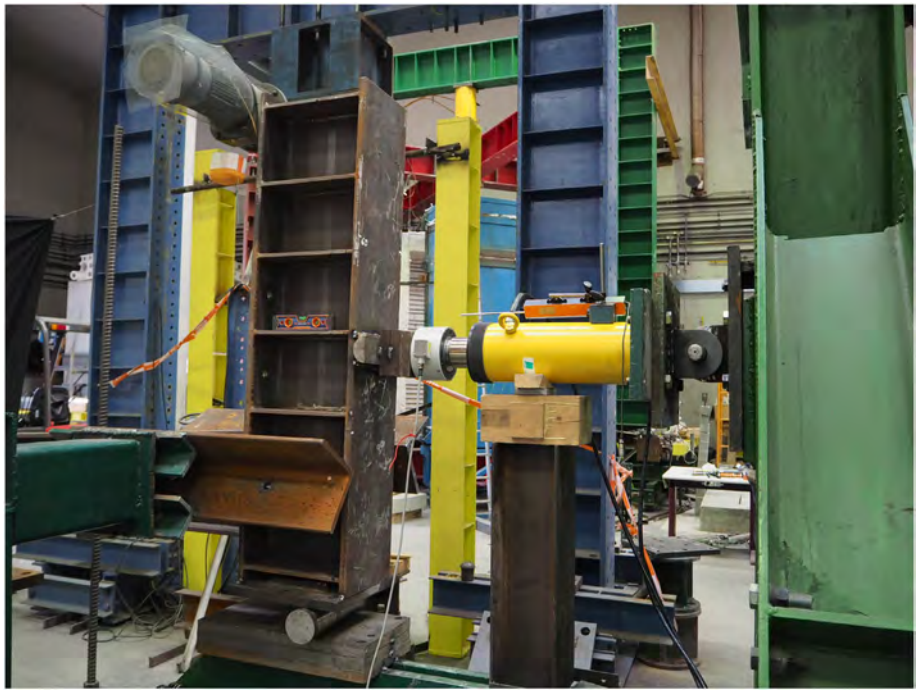

Fig. 8. Point of load application.

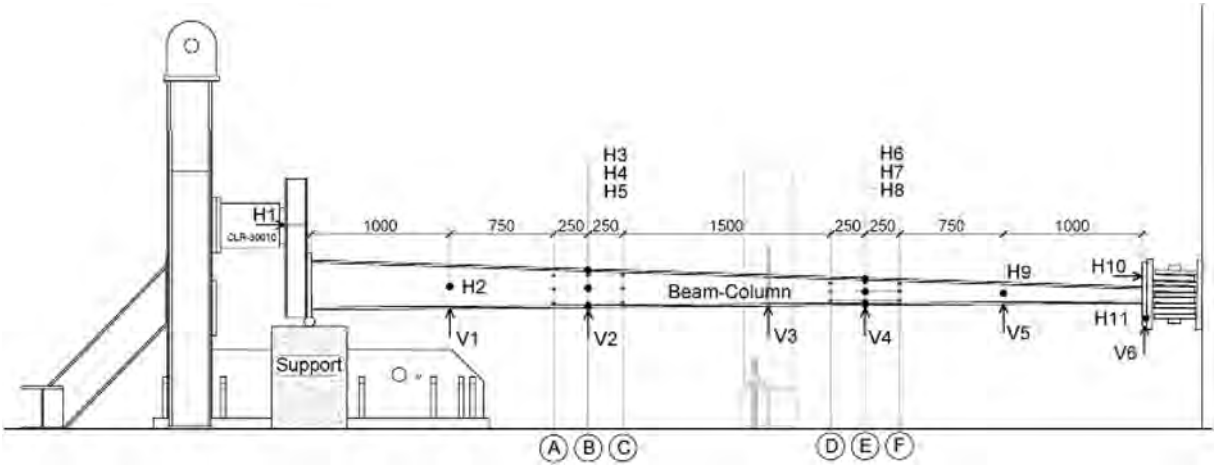

Fig. 9. Test layout.

webs, according to EN ISO 377 [37] and ISO 6892-1 [38]. The value of the yield stress f_y is taken as the upper yield strength R_{eH} and the tensile strength R_m. is used for the ultimate strength f_u. The yield and ultimate stresses are reported for each specimen according to the plate thickness, i.e. for specimens having different thicknesses in the web and in the flanges, the results are reported separately. The Young's modulus is calculated as an average from all tests performed per specimen. The results are summarized in Table 3.

3.3.2. Measurement of geometrical imperfections

The geometrical imperfections may be of different natures (Fig. 10) and they can all influence the buckling behaviour of slender members. For each member, the depths of the deep and shallow cross-sections were measured as well as the web and flange thicknesses at various locations along the member length. Furthermore, the initial global out-of-straightness was measured for all members except Column 2.

The measurement procedure involved a “low mass” nylon string which was tied to two nuts at the member's extremities and it was stretched to its maximum. The distance of the string to the member was then measured at each 0.50 m length. To obtain the magnitude of the imperfection the nuts height was subtracted. The measurement was performed for three lines along the member web and one for each flange. The magnitude of the geometrical imperfection was considered as an average of the measurements.

Table 3
Material properties from tensile coupon tests.

Specimen	C1	C2		C3		BC	
Location	–	Flange	Web	Flange	Web	Flange	Web
f_y	376.7	371.3	362.1	385.5	450.8	391.9	443.1
f_u	570.3	571.0	507.4	535.4	595.3	540.4	588.8
E	208.1	213.1		206.0		210.2	

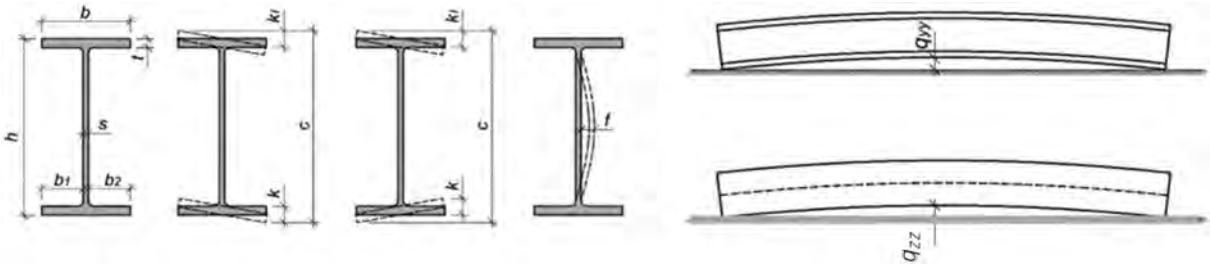

Fig. 10. Geometrical imperfections.

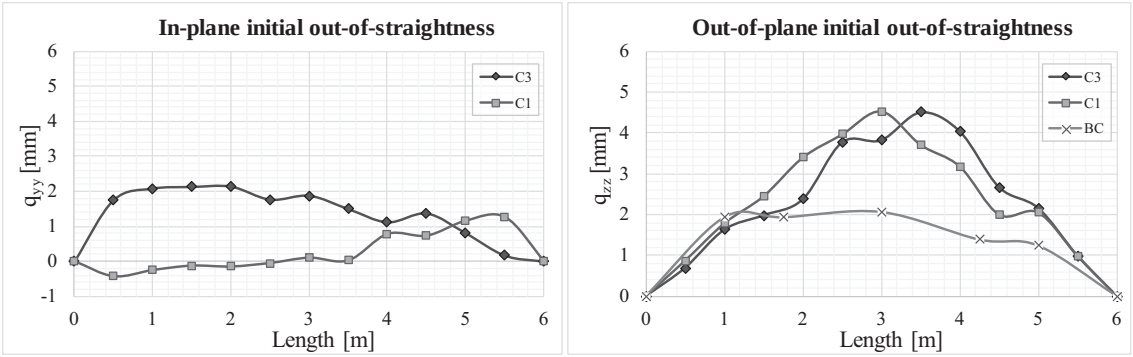

Fig. 11. Initial out-of-straightness.

Even though it is not an advanced measurement method, it allows for an initial idea of the magnitude the imperfections to be used in the numerical models.

The average results obtained for all members are shown on Fig. 11.

3.3.3. Residual stresses

In order to completely characterize the behaviour of the tested specimens, residual stresses measurements were also carried out (Fig. 12).

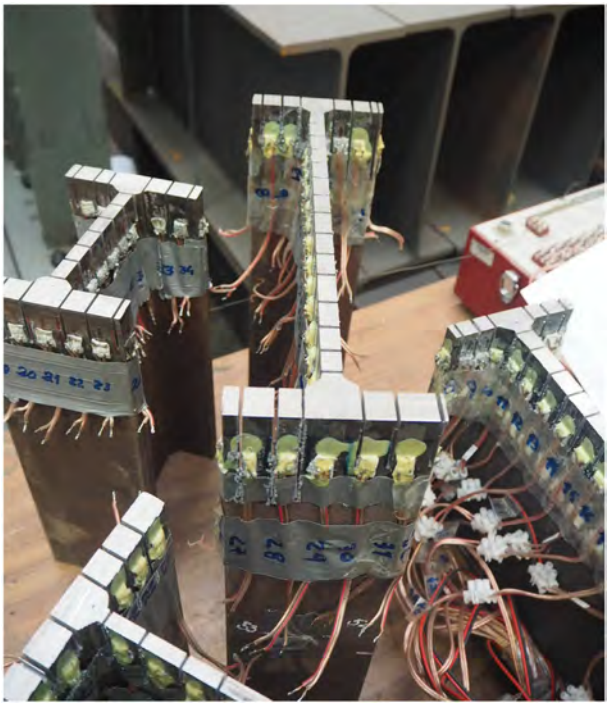

Fig. 12. Specimens after testing.

The measurements were made on test pieces with dimensions representing different regions of the tapered columns and beam-columns corresponding to various tapering ratios and heights. The approximate location of the column segments and the specimen dimensions are given in Fig. 13 and Table 4, respectively. The length of the test pieces was chosen to be about 5 times the height of the measurement cross-section in order to avoid any possible boundary effects in the measurement.

The test procedure followed the sectioning method [25], which is a commonly adopted measurement procedure for structural engineering purposes [27]. The procedure involves longitudinal and transversal cuts which provoke the release of stresses locked in the test specimen, which in turn cause deformations. Then it is possible to record these deformations and transform them further into stresses using Hooke's law [25].

An example of the measurement results is given in Fig. 14 for Column 1 and Column 3.

3.4. Loading protocol

For each column, the loading was divided into two stages: firstly, a cycle of loading and unloading (in the elastic range) was applied and, in the second stage, the columns were loaded until failure.

The first loading stage allowed for adjustments in the test layout (test specimen, hinges and reaction frame), and served for the elimination of initial gaps in the test layout.

The initial stage also allowed to verify the functionality of the strain gauges, LVDT's and data logger.

In the first stage, the loading was applied in force control and in the second in displacement control. The speeds used in each test are given in Table 5.

3.5. Results

In this section, the results from the experiments are briefly summarized. The expected failure mode for the three columns was in-plane flexural buckling with local buckling for C2. The beam-column was expected to fail in lateral-torsional buckling.

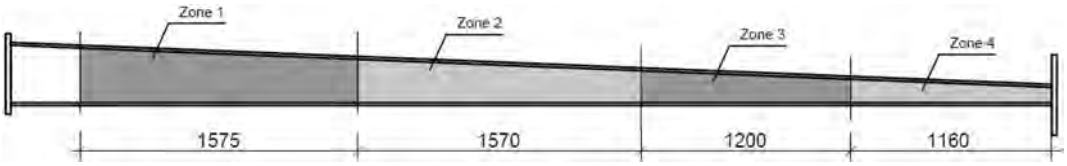

Fig. 13. Location of specimens for the residual stress measurements.

Nevertheless, despite the large number of lateral restraints, Column 1 and Column 2 still buckled out-of-plane in between the lateral restraints almost simultaneously as they reached their in-plane resistance. In the last column test, Column 3, it was possible to observe in-plane flexural buckling. The maximum loads recorded during the experiments are given in Table 6.

Table 4
Specimen dimensions.

Specimen	h_{max}	h_{min}	L
–	mm	mm	mm
RS_1	365	270	1575
RS_2	248	211	1200
RS_5	343	280	1570
RS_6	166	120	1160

3.5.1. Test C1

In this section, the results recorded during the test C1 are summarized. The final deformation of the specimen is shown in Fig. 15. Despite the large number of lateral restraints, C1 still buckled out-of-plane in

Table 5
Loading protocol.

	Load → unload cycles [kN]	Load speed 1st phase	Load speed 2nd phase
C1	0 → 600 → 5	0.5 kN/s	0.003 mm/s
C2	0 → 400 → 5	0.5 kN/s	0.003 mm/s
C3	0 → 400 → 5	0.5 kN/s	0.003 mm/s
BC	0 → 50 → 5	0.25 kN/s	0.0025 mm/s

Table 6
Maximum loads during the experiments.

	C1	C2	C3	BC
P_{max}	1398 kN	1313 kN	1456 kN	379 kN
M_{max}	–	–	–	163 kNm

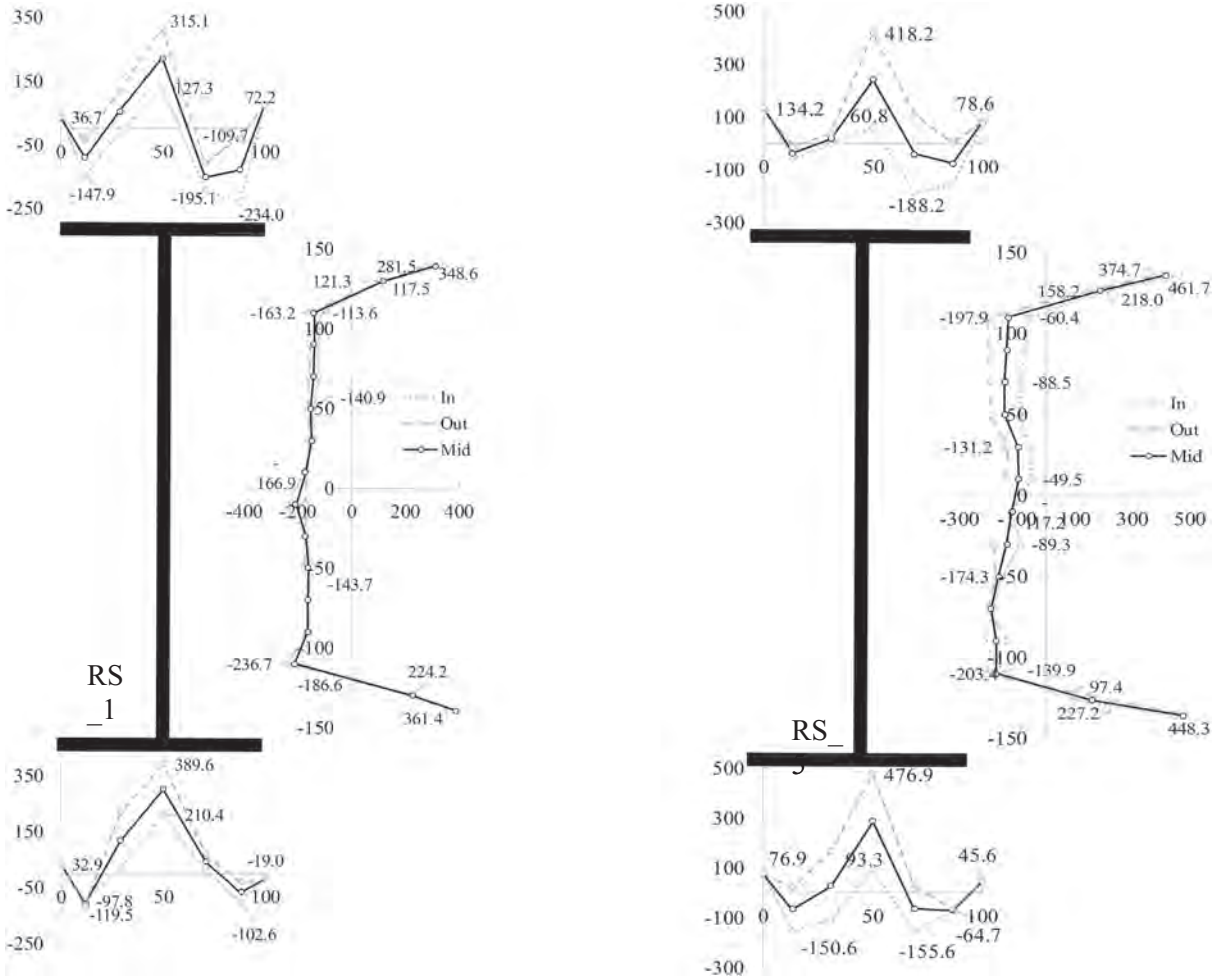

Fig. 14. Measured residual stresses for Column 1 and Column 3.

Fig. 15. Column 1 after the test.

between the lateral restraints almost simultaneously as it reached its in-plane resistance. Also, even though test C1 had a slender cross-section (cross-section class is 4 for 18% of its length), failure was driven by global rather than local instability phenomena.

The column's displacements and strains were monitored at several locations along the member length, aimed to facilitate the subsequent calibration of a numerical model and also to serve as control measurements in order to confirm the reliability of the results.

Fig. 16 illustrates the load-displacement curve at the point of load application (H_1 and H_2). The maximum applied load during the experiment was 1397.6 kN. The loading was stopped when the applied force dropped to approximately $P = 1000$ kN.

It is worth analyzing the vertical displacements along the column. Fig. 17 shows the evolution of the curvature at 200 kN intervals of loading at measurement points V_6 to V_{11}, V_{14} and V_{15}, until the maximum load $P_{ult,Exp}$ and after the maximum load was reached for two additional load steps. The amplification of the initially imperfect shape is clearly visible, which is transformed at higher loads into the in-plane buckled shape. Yet, at the end of the experiment the out-of-plane deformations were more considerable than the in-plane ones.

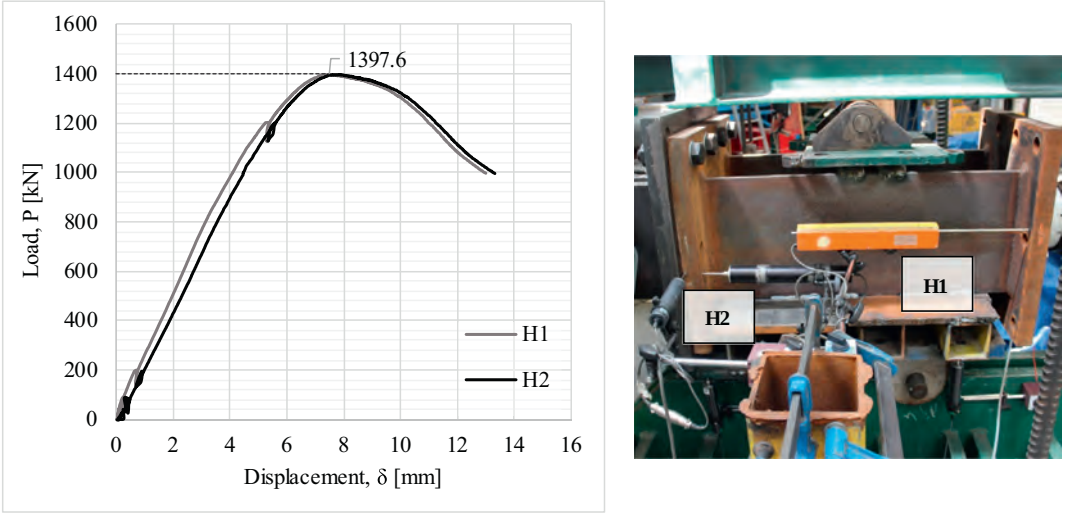

Fig. 16. Load-displacement curves H_1 and H_2 for Column 1.

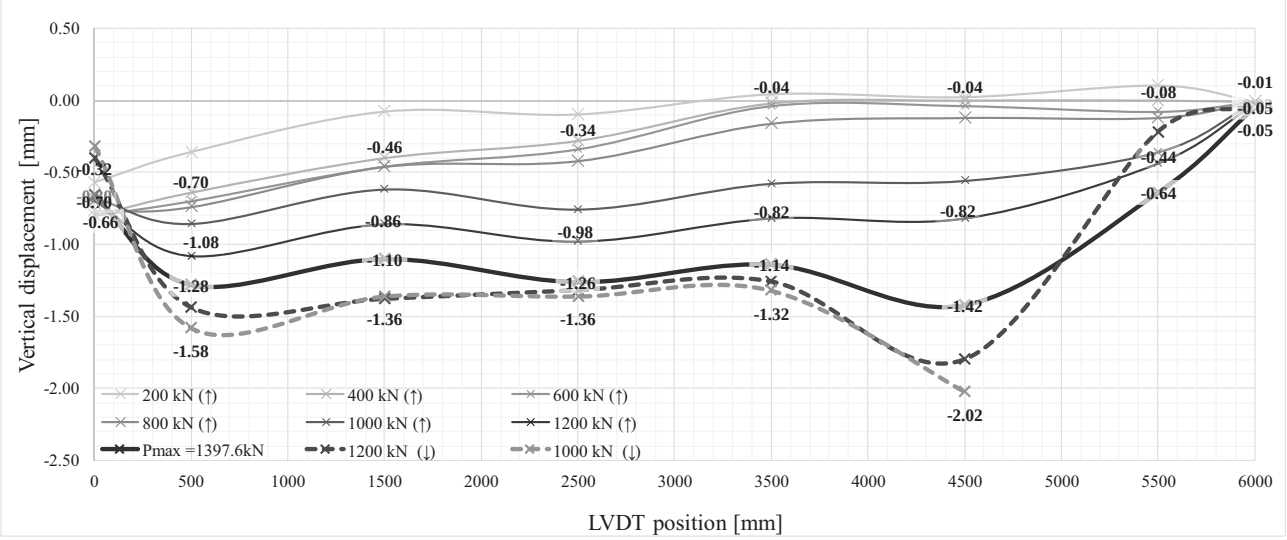

Fig. 17. Variation of the vertical displacements along the C1 with loading.

Furthermore, the stresses were also measured at several cross-sections along the member length. All strains were converted into stresses using the Young's modulus from Table 3, and since all stresses were in compression, a positive sign is used to represent them. Whenever the strains exceeded ε_y, the respective stresses were set equal to the measured yield stress.

The stress evolution for sections A and E are shown in Fig. 18. Section A falls in the Class 3 region; nevertheless, the recorded stress distributions are purely elastic and far from the yield limits given in Table 3. The other cross-section, at axis E, is in Class 1 and being smaller it was subject to higher stresses so that at the maximum load it was fully yielded.

3.5.2. Test C2

The second experiment, C2, was planned for an interaction between global and local buckling. In this case, similarly to C1, the column also buckled in between the lateral restraints. Since more than 85% of the member was in Class 4, it was also possible to observe local buckles on the web towards the deeper cross-section. Fig. 19 illustrates the failure of Column 2.

Fig. 20 shows the load-displacement curve at the point of load application (H_1 and H_2). The maximum applied load during the experiment was 1313.6 kN. The loading was stopped when the applied force dropped to approximately $P = 1000$ kN.

As in-plane buckling was the expected failure mode, the vertical deformations were measured at several locations for C2 as well. Fig. 21 shows the evolution of the curvature at 200 kN intervals of loading at measurement points V_4 to V_{10}, V_{13} and V_{14}, until the maximum load $P_{ult,Exp}$ and after the maximum load was reached for two additional load steps. In this case it is also possible to identify the amplification of the initially imperfect shape which is transformed at higher loads into the in-plane buckled shape. However, this increase at higher loads is found rather small, due to the fact that at the end of the buckled test the column buckled in between the lateral restraints.

The stress evolution for sections B and F are shown in Fig. 22. Section B falls in the Class 4 region, and the local buckling can be seen in the stress distribution for the load levels 1200 kN and the maximum 1313.6 kN. The other cross-section, at axis F, is also classified as Class 4, however closer to the limit with Class 3, and no local deformation were recorded.

3.5.3. Test C3

In this section, the results recorded during the test C3 are summarized. The final deformation of the specimen is shown in Fig. 23. In this experiment, it was possible to observe distinct in-plane flexural

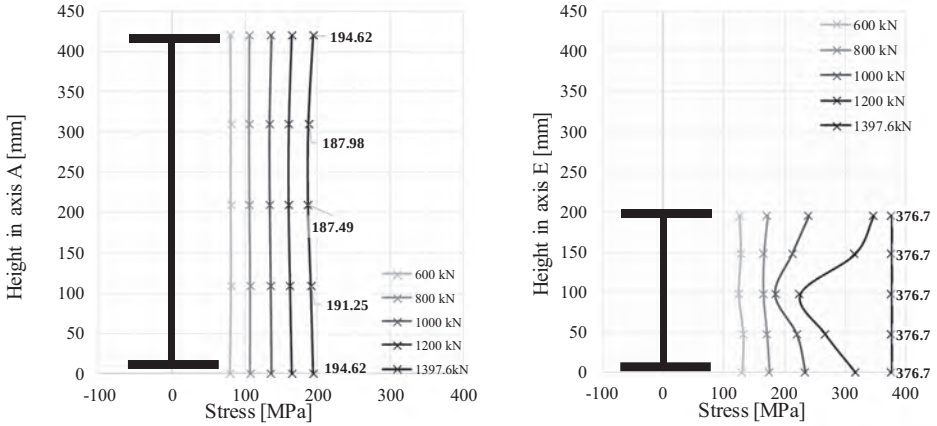

a) Stresses in section A (h = 420mm). *b) Stresses in section E (h = 195mm).*

Fig. 18. Stress distribution at sections A and E for various load levels.

Fig. 19. Collapse of C2.

buckling. The test C3 has a stocky cross-section (cross-section class is 4 for 5% of its length), failure was driven by global rather than local instability phenomena.

Fig. 24 illustrates the load-displacement curve at the point of load application (H_3 and H_2). The maximum applied load during the experiment was 1460 kN. The loading was stopped after the column buckled in-plane, which corresponded to a drop of the load to 800 kN.

Furthermore, Figs. 25 and 26 show the evolution of the curvature for various load levels, where Fig. 26 illustrates the development of the in-plane displacements until the maximum load was recorded. It is very similar to Figs. 17 and 21, where for lower load levels the shape amplifies the initially imperfect one. After the maximum load was achieved, at a force of approximately 1427 kN, C3 buckled in-plane exhibiting an instantaneous increase of the deformations, as shown in Fig. 26.

The stress evolution for sections B and G are shown in Fig. 27. Both cross-sections are in Class 1, no local buckling was registered neither observed during the experiment. However, in both cross-sections it is

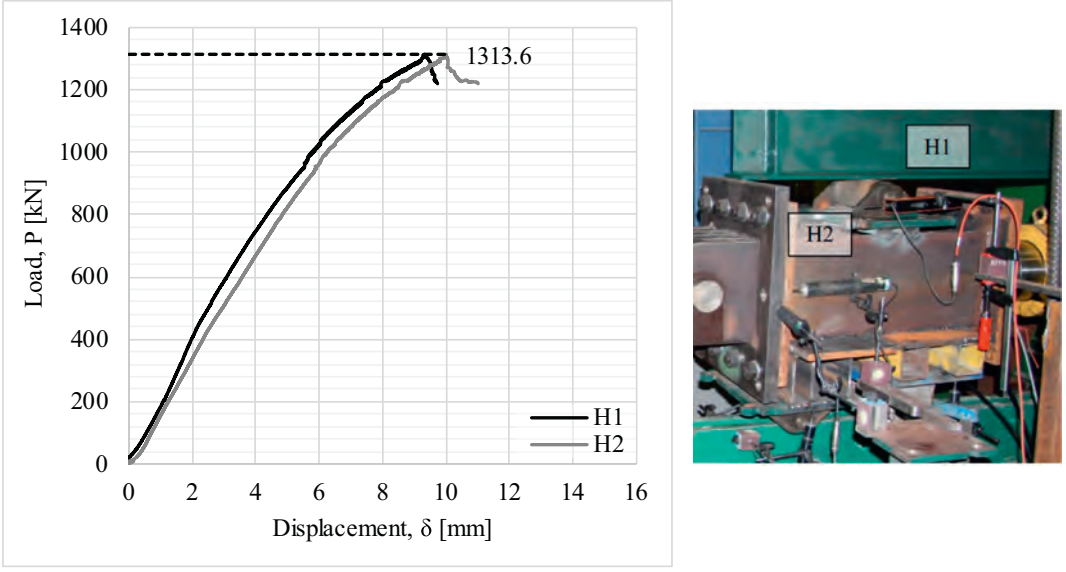

Fig. 20. Load-displacement curves H_1 and H_2 for Column 2.

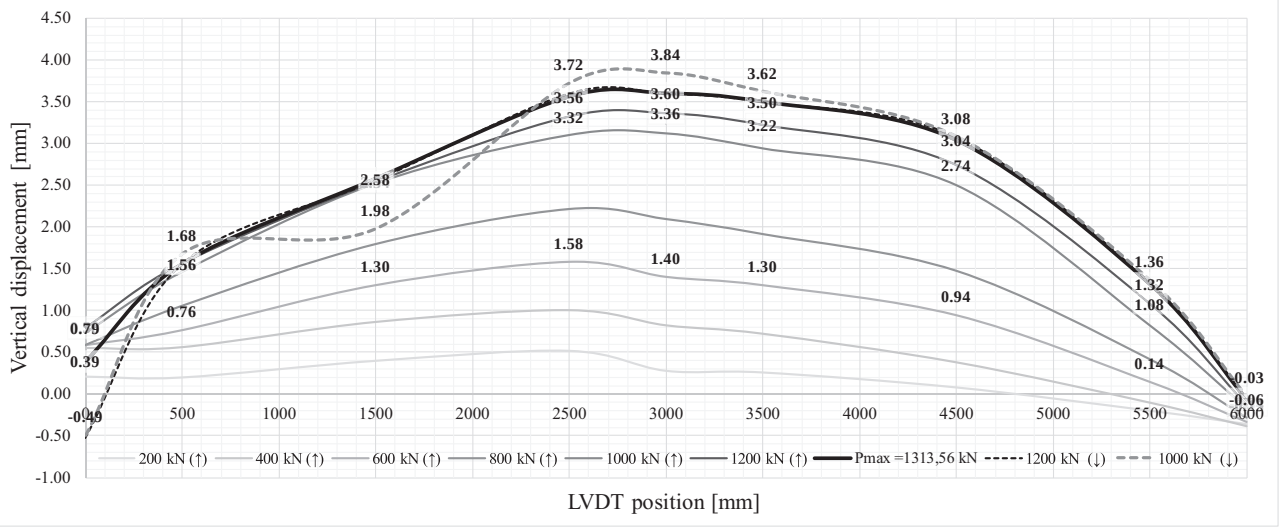

Fig. 21. Variation of the vertical displacements along the C2 with loading.

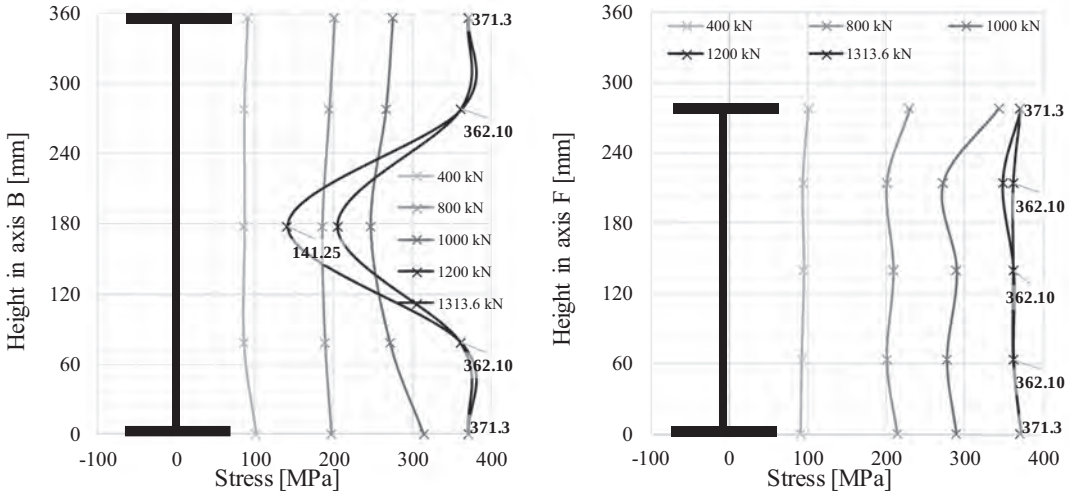

a) Stresses in section B (h = 356mm). b) Stresses in section F (h = 278mm).

Fig. 22. Stress distribution at sections B and F for various load levels.

Fig. 23. Column 3 after the experiment.

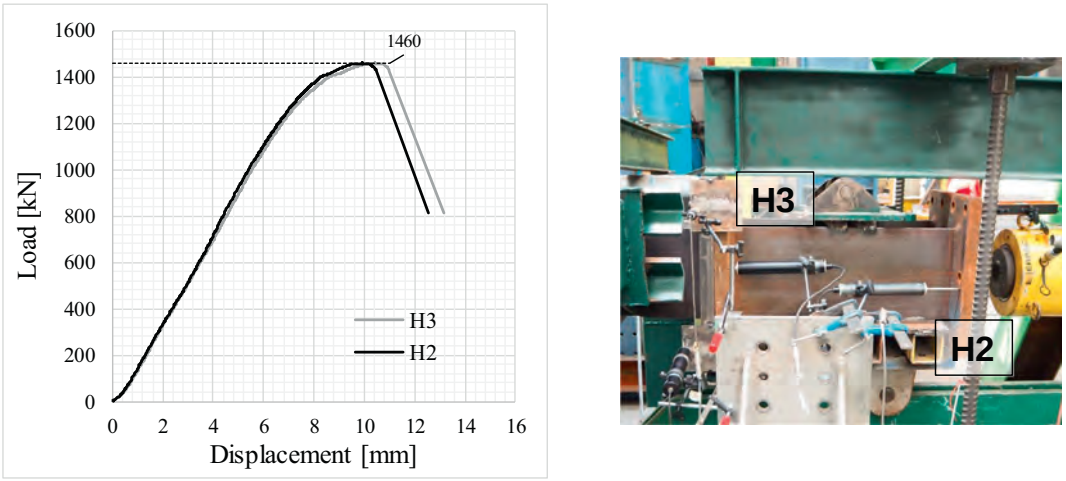

Fig. 24. Load-displacement curves H_3 and H_2 for Column 3.

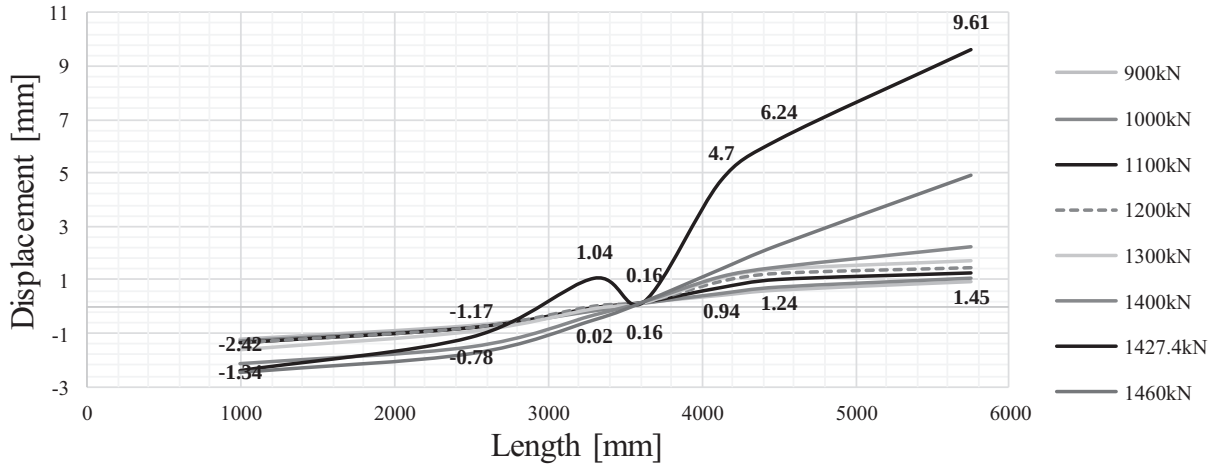

Fig. 25. Variation of the vertical displacements along the C3 with loading.

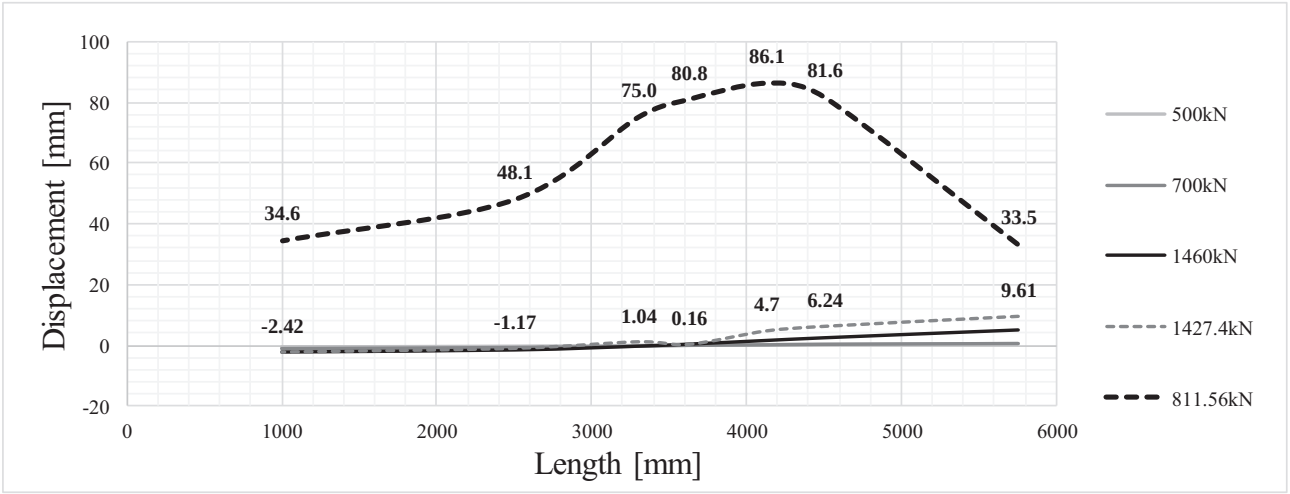

Fig. 26. Variation of the vertical displacements along the C3 beyond maximum load.

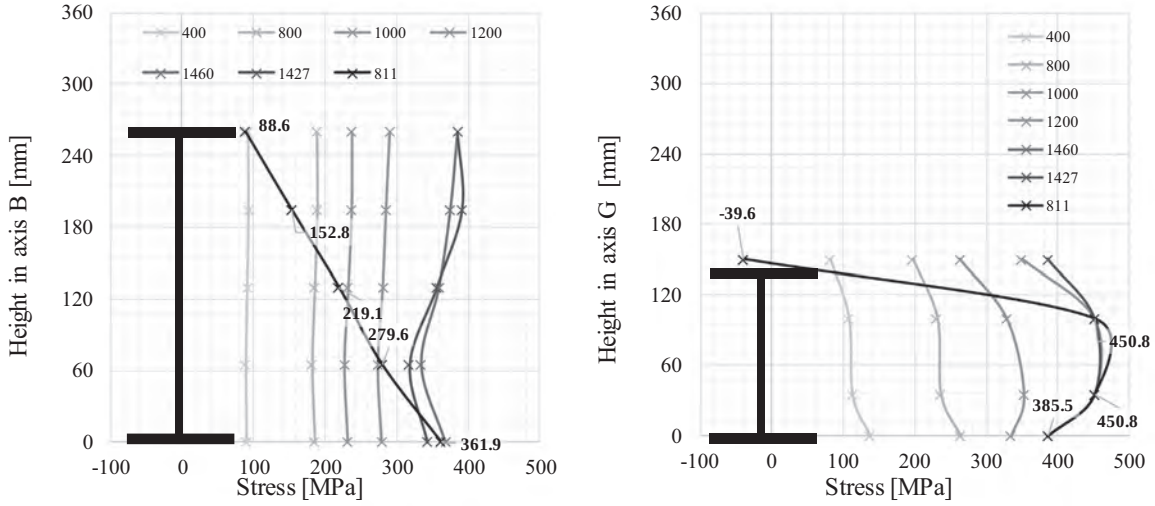

a) Stresses in section B (h = 260mm). *b) Stresses in section G (h = 150mm).*

Fig. 27. Stress distribution at sections B and G for various load levels.

possible to observe the impact of the in-plane buckling behavior. For load levels up to the maximum load the member stresses are mostly in uniform compression; after the buckled position took place at 1427 kN the compressive stresses in the top flanges decrease and in Section G they even become tensile, due to the second order in-plane bending moment.

3.5.4. Test BC

Finally, in this section the results from the beam-column test are summarized. The member had identical geometry as C3, but the axial force was applied with an eccentricity at the deep end of the member, thus introducing a triangular bending moment distribution.

The final deformation of the specimen is shown in Fig. 28. As expected, the specimen collapsed in a lateral-torsional buckling mode. Also, since BC has a stocky section in almost all of its length, failure was driven by global rather than local instability phenomena.

Fig. 29 illustrates the load-displacement curve at the point of load application (H_1). The maximum applied load registered during the experiment was 379 kN corresponding to bending moment equal to 163 kNm. The loading was stopped when the applied force dropped to approximately $P = 270$ kN.

Furthermore, Figs. 30 and 31 show the evolution of the curvature for various load levels. Fig. 30 illustrates the development of the out-of-plane displacements and Fig. 31 the in-plane ones. The dotted line is added to illustrate the expected measurement of the LVDTS at these points. Due to the large deformations the vertical and horizontal LVDTS at this point stopped recording data after the maximum load was reached.

The strains were also recorded at several locations. It is interesting to show the evolution of stresses for axis F (in the middle of the second span), Fig. 32 shows the stress distribution for a few load levels. The resulting distribution at maximum load and after the maximum is typical for lateral-torsional buckling.

4. Numerical model for web-tapered members

Following the experimental results presented in the previous paragraphs, it is the objective here to calibrate a numerical model, which is able to reproduce the real behaviour of web-tapered members.

The numerical modelling techniques adopted in this section are implemented following the same approach as in [2,3]. The model was built using software Abaqus [28]. It includes advanced numerical simulations with geometrical and material imperfections, which are widely adopted for the validation of stability design rules [29]. It is common to adopt a linear 4-node shell element model [2] with material constitutive models either as linear elastic perfectly plastic or as linear elastic with strain hardening, Fig. 33a. The initial geometrical imperfection is usually assumed in the global buckling mode shape for the studied phenomenon with a magnitude of 1/1000 of the member length as shown in Fig. 33b. The material imperfections are accounted for by the residual stress pattern from ECCS recommendation No. 33 [30], as shown in Fig. 33c.

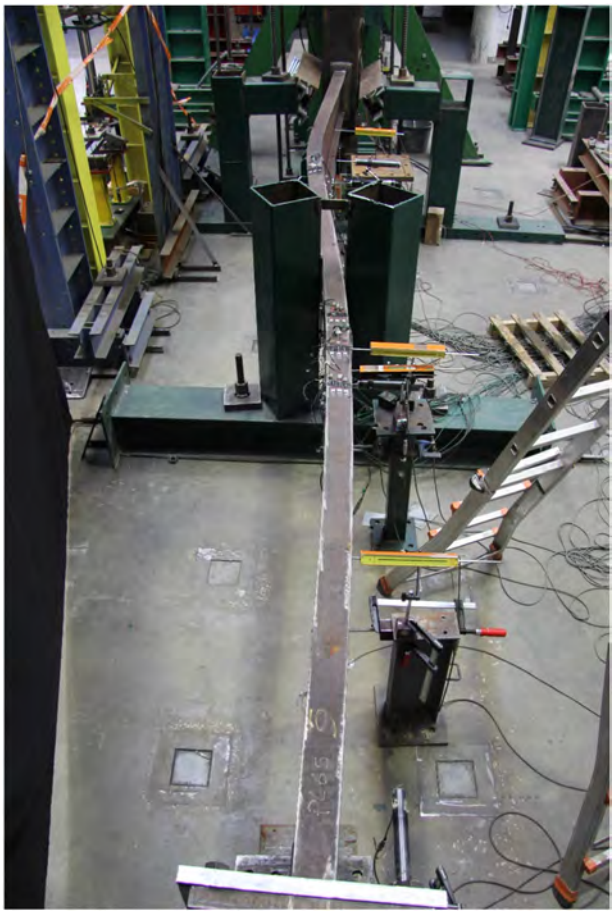

Fig. 28. Deformation of the specimen after the test.

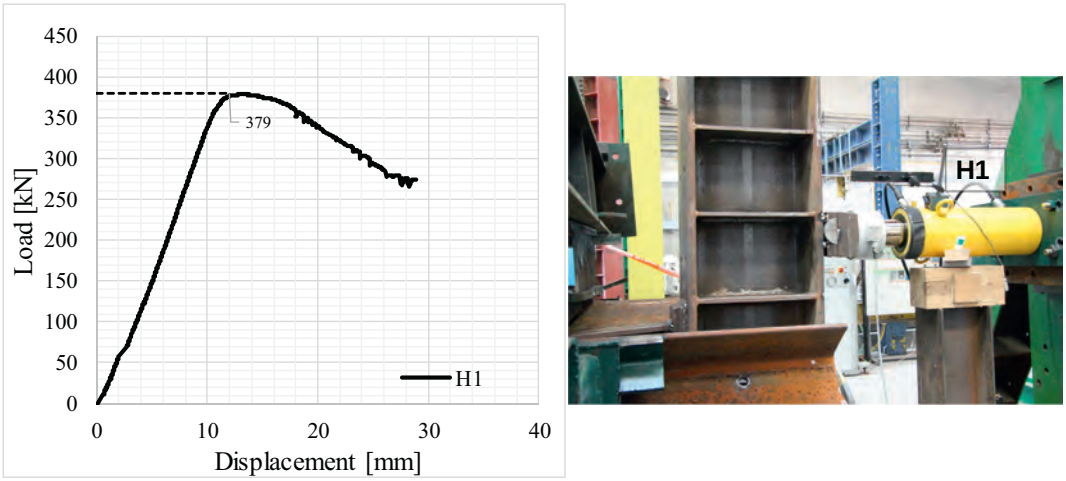

Fig. 29. Load-displacement curves H_1 for BC.

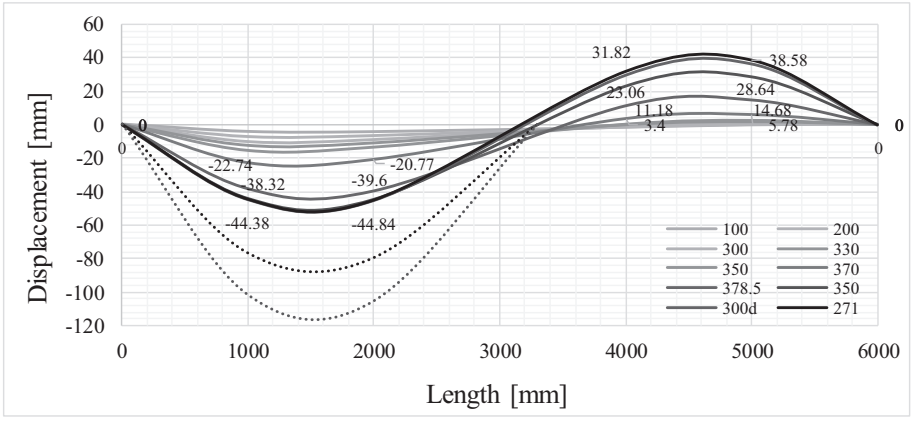

Fig. 30. Out-of-plane displacement.

In order to achieve closer match with the experimental results, a few modifications of the described model were necessary. However, it was also aimed to maintain the model as simple as possible for validation purposes. Firstly, the material properties introduced were according to the results obtained for the coupon tests in Section 3.3.1. About 20 points were chosen from the yield point to the ultimate tensile stress, in the numerical model, those were transformed and introduced as true stresses and logarithmic strains, separately for the flanges and the webs.

The residual stresses were also introduced according to the measurements performed in Section 3.3.3. The flanges were divided into 10 segments and the residual stresses were introduced as an average measured stress for each segment. In the webs the compressive residual stresses were distributed over a distance equivalent to the measured

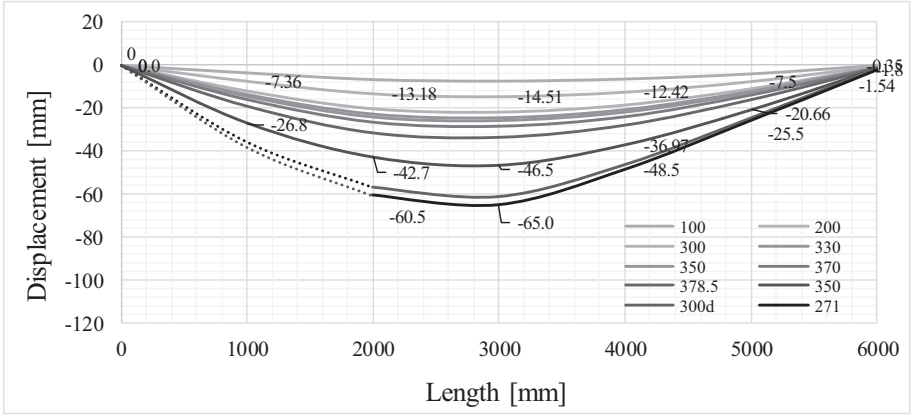

Fig. 31. In-plane displacement.

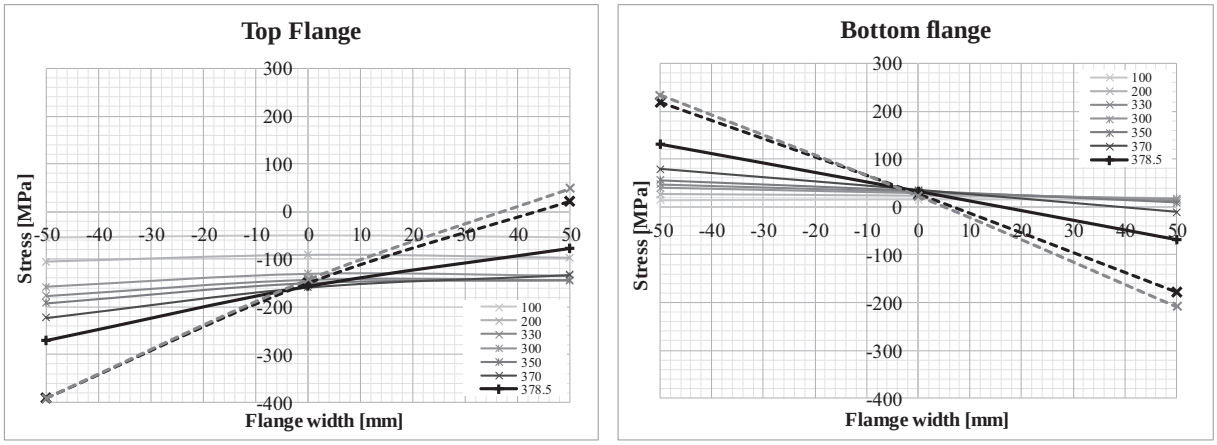

Fig. 32. Stress distribution in the flanges at axis F.

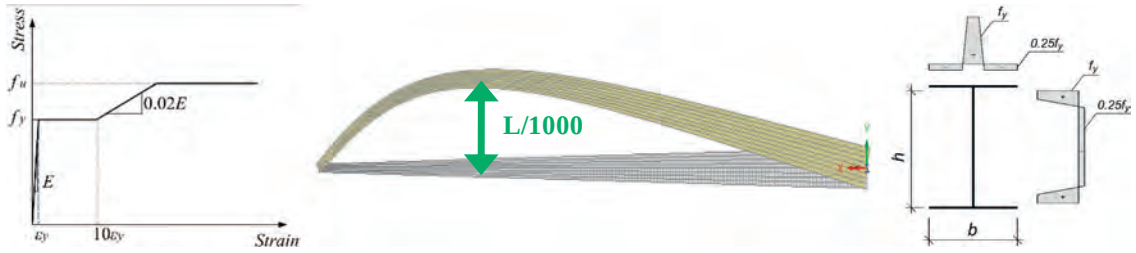

a) constitutive law b) initial geometrical imperfection c) residual stresses pattern

Fig. 33. Model parameters.

a) Column 1 in-plane mode b) Column 1 out-of-plane mode

Fig. 34. Buckling modes as initial imperfection C1.

a) Column 2 in-plane mode b) Column 2 out-of-plane mode

Fig. 35. Buckling modes as initial imperfection C2.

a) Column 3 in-plane mode b) Column 3 out-of-plane mode

Fig. 36. Buckling modes as initial imperfection C3.

with an average stress, while the tensile residual stresses were split into four segments (two at the top and two at the bottom) with the corresponding averages for each test.

The initial geometrical imperfections were modelled as a combination of buckling modes, which resembled the measurement of the geometrical imperfections (as shown in Fig. 10). Several shapes were verified in order to obtain the best fit. For *Column 1*, the adopted imperfection was the combination of a global buckling in-plane mode (Fig. 34a) with an out-of-plane mode including local effects (Fig. 34b).

For *Column 2*, the adopted imperfection was the combination of a global buckling in-plane mode (Fig. 35a) with an out-of-plane mode including local effects (Fig. 35b) with nominal amplitude of L/1000 for the in-plane mode and 2 mm for the local.

For *Column 3*, the adopted imperfection was the combination of a global buckling in-plane mode (Fig. 36a) with an out-of-plane mode including local effects (Fig. 36b).

The boundary conditions were adopted in order to represent the experimental layout Fig. 37. Firstly, the actual buckling length of the members was longer than the actual member length due to the physical dimensions of the supports. To account for this, the boundary conditions were modelled outside of the member at a distance which coincides with the actual axis of rotation of the hinge. The out-of-plane rotations were restrained. The presence of small eccentricities in the layout were included by adding small rotations at the point of load application.

Finally, the resulting load-displacement curves at the point of load application are shown in Fig. 38. In each case, it was possible to achieve satisfactory agreement between the numerical and experimental results in both shape and magnitude. The obtained results and the respective difference between numerical and experimental results are given in Table 7. A comparison between the experimental and numerical deformations can be seen in Fig. 39.

Another important parameter for the design of non-uniform members is the critical cross-section which governs the design. For that, these critical locations obtained from the numerical model and experimental tests are now compared. The experimental critical location was estimated approximately as the cross-section with maximum deformation after the test. The numerical critical location was chosen to correspond to the element with the highest strain at the maximum load. In Table 7, it is possible to compare the experimental and numerical results. Since this quantity is highly dependent on the member imperfections, an exact match can be hardly achieved, even though, the obtained results show very good agreement.

5. Design resistance for web-tapered members

In the previous sections, a summary of experimental tests and advanced numerical modelling of web-tapered columns and beam-columns was described. However, in real design it is not always possible to verify the solution by adopting these approaches. According to EN 1993-1-1 [1], the stability analysis of non-uniform members, may be verified using the General Method given in clause 6.3.4. However, its applicability is limited and, in some aspects, inconsistent [29] due to difficulties in the choice of imperfection factors, determination of the governing cross-section resistance and interaction between forces.

For the verification of linearly web tapered columns Ayrton-Perry analytical models were derived in [2] based on an equivalent simply-supported segment between effective restraints. The verification format is based on a linear interaction between the first order forces and second order bending moments utilizations, leading to a maximum utilization (and, consequently, to the ultimate load factor) at a certain location, denoted as the second order failure location. In [2], it was shown that

Fig. 37. Column and beam-column models.

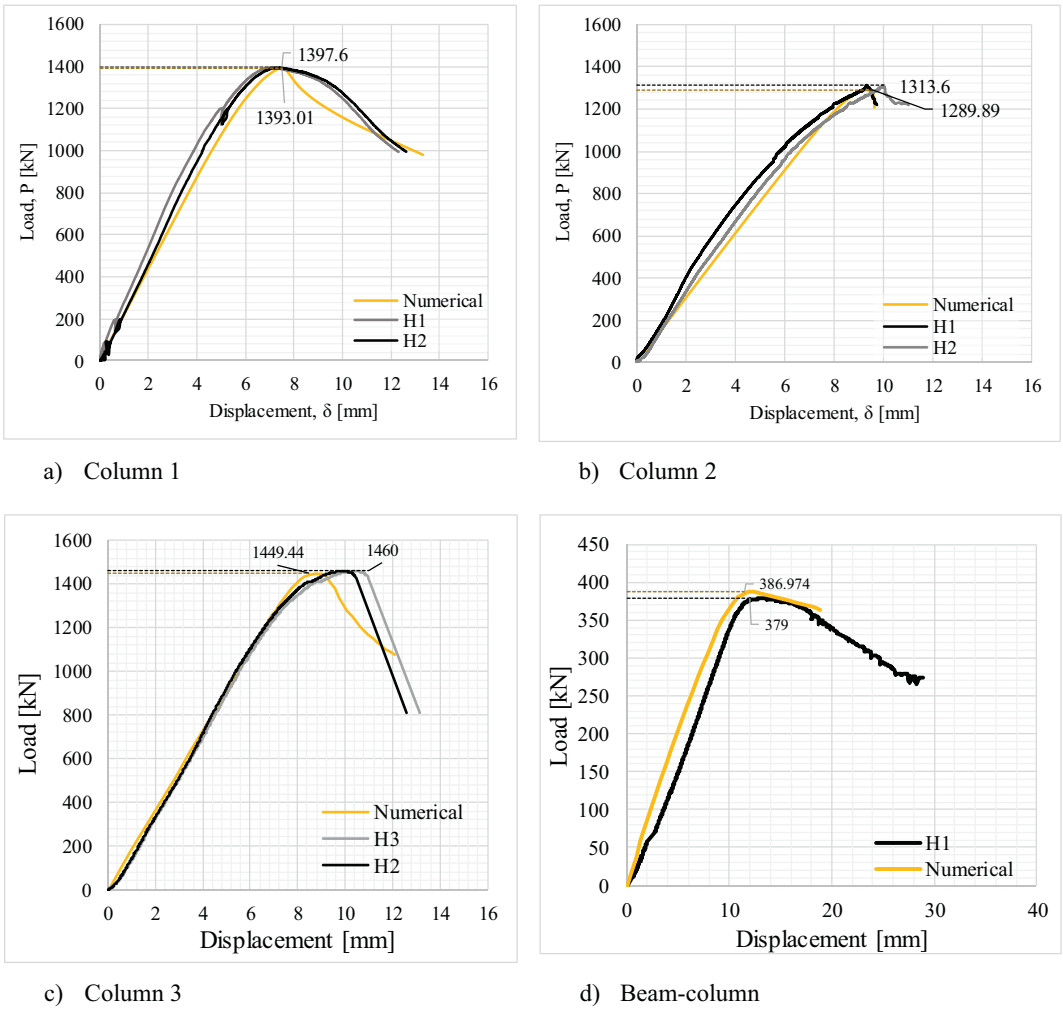

Fig. 38. Numerical and experimental results for each experiment.

Table 7
Numerical and experimental results.

Test	Maximum load		Δ	Critical location x/L	
	Experimental	Numerical		Experimental	Numerical
–	kN	kN	–	–	–
C1	1397.6	**1393.0**	−0.3%	0.110	**0.082**
C2	1313.6	**1289.9**	−1.8%	–	**0.250**
C3	1460.0	**1449.4**	−0.7%	0.125	**0.153**
BC	379.0	**386.9**	+2%	0.708	**0.773**

this second order failure location and additional imperfection factor may be replaced in some of the terms by an "over-strength" factor φ which accounts for the relation between the ultimate resistance multiplier of the second order location, $\alpha_{ult,k}(x_c^{II})$ and the first order location, $\alpha_{ult,k}(x_c^{I})$. Furthermore, as mentioned earlier, the design rules for tapered columns and beams developed in [2,3] were used to propose a verification format for the stability verification of web-tapered beam-columns [5] by adjusting the k_{yy} and k_{zy} factors of the EC3 interaction formula. The extension was achieved by the consideration of the normalized slenderness about the major or minor axes with the geometrical properties of the previously calibrated second order failure location

Fig. 39. Column 3: numerical and experimental deformed shape.

Table 8
Numerical and experimental results.

Test	Maximum load			Critical location x/L		
	Experimental	Numerical	Analytical	Experimental	Numerical	Analytical
–	kN	kN	–	–	–	
C1	1397.6	1393.0	1311.7	0.110	0.082	0.129
C2	1313.6	1289.9	1172.9	–	0.250	0.260
C3	1460.0	1449.4	1244.8	0.125	0.153	0.196
BC	379.0	386.9	275	0.708	0.773	–

(Table 9) and the interaction formula applied at the first order failure location (Eqs. (8) and (9)).

$$\frac{N_{Ed}\left(x^{I}_{c,N}\right)}{\chi_y\left(x^{I}_{c,N}\right)N_{Rk}\left(x^{I}_{c,N}\right)/\gamma_{M1}} + k_{yy}\frac{M_{y,Ed}\left(x^{I}_{c,M}\right)}{\chi_{LT}\left(x^{I}_{c,M}\right)M_{y,Rk}\left(x^{I}_{c,M}\right)/\gamma_{M1}} \le 1.0 \quad (8)$$

$$\frac{N_{Ed}\left(x^{I}_{?}\right)}{\chi_z\left(x^{I}_{c,N}\right)N_{Rk}\left(x^{I}_{c,N}\right)/\gamma_{M1}} + k_{zy}\frac{M_{y,Ed}\left(x^{I}_{c,M}\right)}{\chi_{LT}\left(x^{I}_{c,M}\right)M_{y,Rk}\left(x^{I}_{c,M}\right)/\gamma_{M1}} \le 1.0 \quad (9)$$

Both methods were applied to the columns and the beam-column, leading to the design resistances and critical locations presented in Table 8. When these results are compared to the experimental ones they are all safe-sided estimates of the registered resistance during the tests. In all cases, the design resistances are slightly safer, this is explained by the assumptions when calibrating the design method such as residual stresses and geometrical imperfection, but also the incorporated safety in the design rule accounting for the variability of all basic variables [31]. A summary of the obtained results is given in Fig. 40. The estimated critical locations from the design method are also very close to the experimental and numerical predictions.

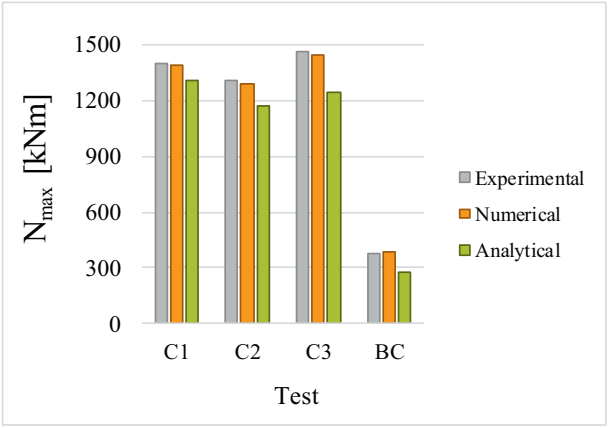

Fig. 40. Comparison between experimental, numerical and analytical.

Table 9
Interaction factors for web-tapered beam-columns according to Method 2.

k_{yy}	$C_{my}\times\left(1+\left(\overline{\lambda}_y\left(x^{II}_{c,N}\right)-0.2\right)\le 0.8 \ \ge 0 \ \frac{N_{Ed}\left(x^{I}_{c,N}\right)}{\chi_y\left(x^{I}_{c,N}\right)N_{Rk}\left(x^{I}_{c,N}\right)/\gamma_{M1}}\right)$
k_{zy}	$1-\frac{0.1\overline{\lambda}_z\left(x^{II}_{c,N}\right)}{C_{m,LT}-0.25}\frac{N_{Ed}\left(x^{1}_{c,N}\right)}{\chi_z\left(x^{1}_{c,N}\right)N_{Rk}\left(x^{1}_{c,N}\right)/\gamma_{M1}}$ ≤ 0.1 $for\ \overline{\lambda}_z\left(x^{II}_{c,N}\right)<0.4$:$0.6+\overline{\lambda}_z\left(x^{II}_{c,N}\right)\le 1-\frac{0.1\overline{\lambda}_z\left(x^{II}_{c,N}\right)}{C_{m,LT}-0.25}\frac{N_{Ed}\left(x^{1}_{c,N}\right)}{\chi_z\left(x^{1}_{c,N}\right)N_{Rk}\left(x^{1}_{c,N}\right)/\gamma_{M1}}$

6. Conclusions

In summary, this paper presented four full-scale experimental tests on the stability behaviour of linearly web-tapered steel columns and beam-column. The columns were tested under constant axial force aiming for the assessment of their in-plane flexural buckling resistance and one member was tested under bending and axial force. The material and geometrical properties of all members were characterized experimentally and detailed global results were reported. The test campaign also included residual stresses tests, where four specimens with different geometries were tested.

The member geometrical properties were chosen to vary from stocky cross-sections to columns with slender (class 4) cross-sections, and therefore, they provide a good basis for their use as reference tests for the calibration and validation of numerical models.

Moreover, it was demonstrated that the commonly adopted numerical model for stability of steel members, as described in [2,3] is adequate of reproducing the experimental results if the real geometrical, material properties and imperfections are considered, together with a correct representation of the boundary conditions. Therefore, as this numerical model is supported by the experimental tests presented in this paper, it can be recommended as a good basis future development in the area of stability design.

Finally, the experimental results provide additional physical validation of the design method proposed in [2] for web-tapered columns.

Acknowledgments

The research leading to these results has received funding from:

- the Portuguese Foundation for Science and Technology (FCT) under grant agreement TAPERSTEEL PTDC/ECM-EST/1970/2012.
- the Portuguese Foundation for Science and Technology (FCT) under grant agreement SFRH/BD/99702/2014
- This work was partly financed by FEDER funds through the Competitivity Factors Operational Programme - COMPETE and by national funds through FCT – Foundation for Science and Technology within the scope of the project POCI-01-0145-FEDER-007633

References

[1] Eurocode, EN 1993-1-1, Eurocode 3: Design of Steel Structures - Part 1–1: General Rules and Rules for Buildings CEN, Brussel, 2005.
[2] L. Marques, A. Taras, L. Simões da Silva, R. Greiner, C. Rebelo, Development of a consistent design procedure for tapered columns, J. Constr. Steel Res. 72 (2012) 61–74.
[3] L. Marques, L. Simões da Silva, R. Greiner, C. Rebelo, A. Taras, Development of a consistent design procedure for lateral-torsional buckling of tapered beams, J. Constr. Steel Res. 89 (2013) 213–235.
[4] T.V. Galambos, Guide to Stability Design Criteria for Metal Structures, Fifth Edition John Wiley & Sons Inc, 1998.
[5] L. Marques, L. Simões da Silva, C. Rebelo, A. Santiago, Extension of EC3-1-1 interaction formulae for the stability verification of tapered beam-columns, J. Constr. Steel Res. 100 (2014) 122–135.
[6] S.P. Timoshenko, J.M. Gere, Theory of Elastic Stability, 2nd Edition McGraw-Hill, New York, 1961 ISBN: 0070647496.
[7] J.C. Ermopoulos, Buckling of tapered bars under stepped axial loads, J. Struct. Eng. ASCE 112 (6) (1986) 1346–1354.
[8] G.C. Lee, M.L. Morrell, R.L. Ketter, Design of tapered members, Weld Res. Counc. Bull. No. 173, June 1972, pp. 1–32.

[9] J.B. Salter, D. Anderson, I.M. May, Tests on tapered steel columns, The Structural Engineer, Vol. 58A, 1980, pp. 189–193.
[10] J.C. Ermopoulos, Equivalent buckling length of non-uniform members, J. Constr. Steel Res. 42 (2) (1997) 141–158.
[11] R.H. Wood, Effective lengths of columns in multi-storey buildings, The Structural Engineer, 52(7–8–9), , 1974 pp. 235-295-241.
[12] M.A. Hirt, M. Crisinel, Charpentes Métaliques – Conception et Dimensionnement des Halles et Bâtiments, Traité de Génie Civil, vol. 11, Press Polytechniques et Universitaires Romandes, Lausanne, 2001.
[13] A.M. Baptista, J.P. Muzeau, Design of tapered compression members according to Eurocode 3, J. Constr. Steel Res. 46 (1998) 146–148.
[14] I.G. Raftoyiannis, J.C. Ermopoulos, Stability of tapered and stepped steel columns with initial imperfections, Eng. Struct. 27 (2005) 1248–1257.
[16] J. Naumes, Biegeknicken und Biegedrillknicken von Stäben und Stabsystemen auf einheitlicher GrundlagePhD thesis RWTH Aachen, Germany, 2009.
[17] Y.D. Kim, Behaviour and Design of Metal Building Frames Using General Prismatic and Web-tapered Steel I Section MembersPhD thesis Georgia Institute of Technology, 2010.
[18] AISC, American Institute of Steel Construction, Specification for Structural Steel Buildings, Chicago, Illinois, USA, 2010.
[19] D. Butler, G. Anderson, The elastic buckling of tapered beam-columns, Welded Research Supplement 1963, pp. 29–36.
[20] S. Prawel, M. Morell, G. Lee, Bending and buckling strength of tapered structural members, Welding Research Supplement 1974, pp. 75–84.
[21] H. Shiomi, M. Kurata, Strength formula for tapered beam-columns, J. Struct. Eng. 110 (1984) 1630–1643.
[22] S.L. Chan, Buckling analysis of structures composed of tapered members, J. Struct. Eng. 116 (7) (1990) 1893–1906.
[23] H.R. Ronagh, M.A. Bradford, M.M. Attard, Nonlinear analysis of thin-walled members with variable cross-section. Part I: theory, Comput. Struct. 77 (2000) 285–299.
[24] H.R. Ronagh, M.A. Bradford, M.M. Attard, Nonlinear analysis of thin-walled members with variable cross-section. Part II: application, Comput. Struct. 77 (2000) 301–313.
[25] S.W. Liu, R. Bai, S.L. Chan, Y.P. Liu, Second order direct analysis of domelike structures consisting of tapered members with I-sections, J. Struct. Eng. 142 (5) (2016), 4016009;
N. Tebedge, G. Alpsten, L. Tall, Residual-stress measurement but the sectioning method, Exp. Mech. (1973) 88–96.
[27] R.C. Spoorenberg, H.H. Snijder, J.C.D. Hoenderkamp, Experimental investigation of residual stresses in roller bent wide flange steel sections, J. Constr. Steel Res. 66 (2010) 737–747.
[28] Abaqus, v.6.17, Dassault Systems/Simulia, Providence, RI, USA, 2017.
[29] L. Simões da Silva, L. Marques, C. Rebelo, Numerical validation of the general method in EC3-1-1 for prismatic members, J. Constr. Steel Res. 66 (4) (2010) 575–590.
[30] Brussels ECCS, Ultimate Limit State Calculation of Sway Frames With Rigid Joints. ECCS, Technical Committee, Publication No. 33, 1984.
[31] T. Tankova, L. Simões da Silva, M. Marques, C. Rebelo, A. Taras, Towards a standardized procedure for the safety assessment of stability design rules, J. Constr. Steel Res. 103 (2014) 290–302.
[32] CEN, EN 10025-2:2004. Hot Rolled Products of Structural Steels - Part 2: Technical Delivery Conditions for Non-alloy Structural Steels, European Committee for Standardisation, Brussels, 2004.
[33] CEN, EN 15048-1:2007. Non-preloaded Structural Bolting Assemblies – Part1: General Requirements, European Committee for Standardisation, Brussels, 2007.
[34] ISO, EN ISO 4017:2000. Hexagon Head Screws. Product Grades A and B, International Organization for Standardization, 2000.
[35] ISO, EN ISO 4032:2000. Hexagon Nuts, Style 1. Product grades A and B, International Organization for Standardization, 2000.
[36] ISO, EN ISO 7089:2000. Plain washers – Normal series – Product grade A, International Organization for Standardization, 2000.
[37] ISO, EN ISO 377:2013. Steel and Steel Products - Location and Preparation of Samples and Test Pieces for Mechanical Testing, International Organization for Standardization, 2013.
[38] CEN, EN ISO 6892-1:2009. Metallic Materials - Tensile Testing - Part 1: Method of Test at Room Temperature, European Committee for Standardisation, Brussels, 2009.